PCCP

Dynamic Article Links

Cite this: *Phys. Chem. Chem. Phys.*, 2011, **13**, 16644–16654

www.rsc.org/pccp

PAPER

First principles scheme to evaluate band edge positions in potential transition metal oxide photocatalysts and photoelectrodes

Maytal Caspary Toroker,[a] Dalal K. Kanan,[b] Nima Alidoust,[c] Leah Y. Isseroff,[d] Peilin Liao[b] and Emily A. Carter*[ae]

Received 29th June 2011, Accepted 26th July 2011
DOI: 10.1039/c1cp22128k

The positions of electronic band edges are one important metric for determining a material's capability to function in a solar energy conversion device that produces fuels from sunlight. In particular, the position of the valence band maximum (conduction band minimum) must lie lower (higher) in energy than the oxidation (reduction) reaction free energy in order for these reactions to be thermodynamically favorable. We present first principles quantum mechanics calculations of the band edge positions in five transition metal oxides and discuss the feasibility of using these materials in photoelectrochemical cells that produce fuels, including hydrogen, methane, methanol, and formic acid. The band gap center is determined within the framework of DFT + U theory. The valence band maximum (conduction band minimum) is found by subtracting (adding) half of the quasiparticle gap obtained from a non-self-consistent GW calculation. The calculations are validated against experimental data where possible; results for several materials including manganese(II) oxide, iron(II) oxide, iron(III) oxide, copper(I) oxide and nickel(II) oxide are presented.

1. Introduction

Progress in seeking sustainable and cost effective alternative energy sources is accelerating, especially in the solar energy arena. Significant improvements in solar energy conversion devices require the discovery and/or design of new materials. To date, no material has yet been found that is both cheap and sufficiently efficient for use in the three typical solar energy conversion devices: photovoltaics, photoelectrochemical cells, and photocatalysts.[1] These devices share common physical mechanisms in the initial stages of energy conversion: photon absorption to produce electronically excited states consisting of electron-hole pairs, followed by electron-hole pair separation and transport to ultimately produce either current or fuel in subsequent steps.[2] A variety of material properties affect the efficiency of all three solar energy conversion devices,[3,4] including the band gap for photon absorption, the electron-hole pair lifetime and the electron and hole mobilities. Additionally, for solar fuel production, redox reactions at the material surface are favorable thermodynamically only if the position of conduction band minimum (CBM), denoted by E_{CBM}, or valence band maximum (VBM), denoted by E_{VBM}, lie above or below, respectively, the redox reaction free energies. Consequently, accurate methods for determining band edge positions, either from experiment or theory, are needed. Knowledge of the band edge positions provides the first test that a material must pass to be a potentially effective photoelectrode or photocatalyst.

First-row transition metal oxides (TMOs) are attractive candidates for solar energy applications due to their low cost, relative abundance, stability under exposure to ultraviolet light and resistance to corrosion.[5] The need for accurate calculations of the band positions for TMOs is especially significant in view of the difficulties of experimentally measuring their band edges, which is reflected in the limited number of experimental studies on these materials.[6–12] The placement of band edges are usually determined by photoemission spectroscopy experiments, but charging and defects at the surface of TMOs may lead to inaccuracies in the measurement.[13] In addition, the precise location of the onset of the band edge line shape is often not well defined.[14] The Kelvin probe experiment may also be used to measure the Fermi energy, but does not give a complete description of the material's electronic structure, such as the position of the band edges relative to the Fermi energy.[15]

[a] *Department of Mechanical and Aerospace Engineering, Princeton University, Princeton, New Jersey 08544-5263*
[b] *Department of Chemistry, Princeton University, Princeton, New Jersey 08544-5263*
[c] *Department of Electrical Engineering, Princeton University, Princeton, New Jersey 08544-5263*
[d] *Department of Chemical and Biological Engineering, Princeton University, Princeton, New Jersey 08544-5263*
[e] *Department of Program in Applied and Computational Mathematics and Gerhard R. Andlinger Center for Energy and the Environment, Princeton University, Princeton, New Jersey 08544-5263. E-mail: eac@princeton.edu*

Theoretical calculations of the electronic structure of TMOs, from which the band energies can be extracted, are challenging as well. One source of difficulty is the strong interactions between open shell electrons localized in d orbitals, especially for first row mid-to-late TMOs. Conventional implementations of density functional theory (DFT) using approximate local or semilocal density functionals for electron exchange–correlation (XC) are inappropriate for characterizing these TMOs, exhibiting egregious failures such as incorrectly predicting some of these materials to be metals where they are in fact semiconductors or insulators.[16] The failure is largely due to self-interaction error in the approximate exchange functional; hence some exact Hartree–Fock exchange is often introduced to ameliorate much of the error. This can be done with a hybrid XC functional that includes a portion of exact exchange calculated from the Kohn–Sham (KS) single determinant solution. However, this method is extremely computationally expensive due to the evaluation of nonlocal exchange integrals.[17–19] An alternative and more economical approach is offered by DFT + U theory, which incorporates effective intra-atomic Coulomb (U) and exchange (J) terms by introducing one (U-J) parameter[20,21] that can, *e.g.*, be computed fully *ab initio* from unrestricted Hartree–Fock (UHF) calculations.[22,23] We employ this *ab initio* DFT + U theory in most cases here.

The position of the valence band edge of TMOs may be determined from DFT calculations that include such XC functionals. In practice, however, the band energies computed with KS-DFT are shifted due to the contribution of the pseudopotential (which represents the potential due to the nucleus plus core electrons) at zero momentum vector when employing periodic boundary conditions.[24] Therefore, the positions of KS eigenvalues with respect to the vacuum level can be obtained using a periodic cell model containing a slab representing a semi-infinite surface and a sufficiently thick vacuum region that eliminates interactions between slab periodic images.[25] The work function ϕ, defined as the minimum energy required to extract an electron from a material, is equal to the energy difference between the Fermi level and the electrostatic potential energy in vacuum. The work function can also be described in terms of the VBM,

$$\phi = |E_{\mathrm{VBM}} + \Delta| \tag{1}$$

where $\Delta = \frac{1}{2}E_g$ for an undoped material. Per convention, all electron energies are referenced to the potential energy in the vacuum region. Specifically, in slab models of semiconductors, the energy of the KS VBM equals the energy of the highest occupied band referenced to the potential energy in vacuum (the latter being set to zero energy as the reference state).

The KS VBM has been calculated in this way for a variety of semiconductors including III–V semiconductors[25] and titanium dioxide.[26] This method has also been applied to determine the relative position of two semiconductors' VBM and the highest occupied molecular orbital of an organic dye in hybrid solar cells.[27] Thus, the VBM of a material is conventionally assumed in the literature to be equal to the KS VBM.[25–28] The CBM may then be determined by adding an energy gap to the KS VBM. The energy gap is usually obtained either experimentally[28] or theoretically from, *e.g.*, a quasiparticle (QP) gap calculation.[26]

This approach of calculating the VBM of a semiconductor from KS-DFT suffers from an error associated with the derivative discontinuity of the XC energy.[29] A theorem proved by Perdew and Levy[29] shows that DFT can only provide a lower limit to the absolute value of the VBM even if the XC functional used is exact, because of the inherent assumption in the KS formalism that the XC functional is energy independent. However, the theorem also shows that DFT is formally exact for calculating the band gap center (BGC), denoted here by E_{BGC}. Therefore, here we calculate the BGC based on Perdew and Levy's proof that extends to non-metallic systems Janak's theorem for calculating the work function.[30]

To determine the VBM and CBM from E_{BGC}, the energy gap needs to be computed as well. Although many publications purport to predict band gaps from KS-DFT, such gaps are not directly related to any actual measurements. We refer instead to such gaps as "eigenvalue gaps," since they are merely the difference in KS eigenvalues between the lowest unoccupied and highest occupied states. Because of the lack of derivative discontinuity in the XC functional mentioned above, among a host of other reasons, these KS eigenvalue gaps are not equivalent to either optical or photoemission/inverse photoemission (PES/IPES) gaps and any agreement quoted with respect to experiment is merely fortuitous. By contrast, the many-body Green's function theory known as the GW method has successfully calculated the QP gap of many semiconductor materials.[31] The QP gap is essentially the ionization potential minus the electron affinity of the material, a quantity which is directly comparable to the gap measured by PES/IPES experiments. Hence, we use the GW method, together with the calculated BGC, to determine the VBM and CBM as follows,

$$E_{\mathrm{VBM}} = E_{\mathrm{BGC}} - \tfrac{1}{2}E_g \tag{2a}$$

$$E_{\mathrm{CBM}} = E_{\mathrm{BGC}} + \tfrac{1}{2}E_g \tag{2b}$$

where E_g is the QP gap.

Using the procedure described above, this work presents first principles calculations of the position of band edges for several TMOs that could be promising for solar energy applications, including manganese(II) oxide (MnO), iron(II) oxide (FeO), iron(III) oxide (Fe_2O_3), nickel(II) oxide (NiO), and copper(I) oxide (Cu_2O). Section 2 includes computational details on the BGC and QP gap calculations. Results and discussion of the positions of the VBM and CBM with respect to redox reactions are given in section 3, and concluding remarks are provided in section 4.

2. Computational details

Spin-polarized KS-DFT and DFT + U calculations were performed within the VASP program.[32–34] All materials considered exhibit antiferromagnetic ground states except Cu_2O, which is nonmagnetic; all calculations were carried out with the correct antiferromagnetic spin ordering. Starting geometries for BGC and QP calculations were obtained from calculations that determined the equilibrium lattice vectors and

nuclear positions of the bulk material. The XC functional was chosen for each material based on its accuracy in calculating the material's ground state properties, in particular, the transition metal magnetic moment, the bulk modulus, the lattice constant, the character of the band edge states (*e.g.*, transition metal d-orbitals or oxygen p-orbitals), positions of the d-states relative to the band edges, and the KS eigenvalue gap (although the KS eigenvalue gap does not directly correspond to the measured band gap, it gives some indication as to the nature of the chemical bonds). The DFT + U formalism of Dudarev *et al.*[21] was used for periodic calculations of FeO, Fe_2O_3, and NiO. The local density approximation (LDA) XC functional was used for FeO and the Perdue-Burke-Ernzerhof (PBE) generalized gradient approximation (GGA) XC functional was used for both Fe_2O_3 and NiO. PBE was not used for FeO because it fails to predict the observed elongation of FeO along [111].[23,35] Either LDA or PBE can be used for Fe_2O_3 and NiO because they both yield results that are in agreement with experimental ground state properties.[23,36] The values of the U-J parameters are 3.7, 4.3, and 3.8 eV for FeO (Fe^{2+}),[23] Fe_2O_3 (Fe^{3+}),[23] and NiO (Ni^{2+}),[37] respectively, calculated by our *ab initio* scheme.[23] The value for Ni^{2+} was determined in the same way as reported earlier, namely derived from cluster-size-converged UHF calculations on electrostatically embedded clusters containing up to 43 Ni and 92 O atoms. The HSE XC functional with screening parameter of 0.2 $Å^{-1}$ was used for both MnO and Cu_2O.[17,18]

Projector-augmented wave (PAW) potentials representing the core electrons and nuclei of each atom[38,39] replaced the Mn 1s2s2p3s3p, Fe 1s2s2p3s, Ni 1s2s2p3s3p, Cu 1s2s2p3s3p and O 1s electrons. For late first row transition metals, the core electrons up through the 3p shell are very tightly held and hence are generally subsumed into the frozen core of the PAW potential. Here we did treat the 3p electrons of Fe explicitly, simply to be consistent with earlier bulk and surface iron oxide calculations.[23,40]

The plane wave basis was truncated at a kinetic energy cutoff of 700 eV in all calculations. Gamma-point-centered *k*-meshes were used for all materials. The k-point grid size was $8 \times 8 \times 8$ for MnO and FeO, $4 \times 4 \times 4$ for Fe_2O_3 and $6 \times 6 \times 6$ for NiO and Cu_2O. The bulk unit cells of the antiferromagnetic rocksalt TMOs (MnO, FeO, and NiO) used here are rhombohedral cells containing four atoms. A rhombohedral bulk unit cell also was used for antiferromagnetic Fe_2O_3, containing ten atoms, and a cubic bulk unit cell was used for Cu_2O, containing six atoms. This kinetic energy cutoff for the planewave basis and these *k*-point grids converge the total energy to within 1 meV per atom for all materials. The hybrid functionals included a gamma-point-centered $2 \times 2 \times 2$ *q*-point mesh in the calculation of the Fock potential. The Brillouin zone was integrated with the efficient Gaussian smearing method, using smearing width of 0.01 eV, except for Cu_2O, where the integration was done by the tetrahedron method with Blöchl corrections for greater accuracy.[41–43] Tests showed that Gaussian smearing generally gives the same results as the more accurate tetrahedron method for a small smearing width.

Symmetry was not imposed for primitive cell geometry optimization of bulk FeO to allow for the observed rhombohedral distortion to occur. For bulk MnO, Fe_2O_3, NiO, and Cu_2O, the same structures were obtained whether symmetry was imposed or not, therefore for computational efficiency we imposed symmetry for these four materials. The final lattice constants of the bulk primitive cells calculated with the above selected XC functionals are in good agreement with experimental values and therefore were used for subsequent surface calculations. In particular, the calculated lattice constants for MnO, NiO, and Cu_2O are 5.38 Å, 4.20 Å and 4.29 Å, respectively, compared with experimental values of 5.44 Å,[44] 4.18 Å[45] and 4.27 Å,[46] respectively. The calculated rhombohedral lattice constants for FeO are $|a|$ = 5.25 Å, $|b|$ = 5.25 Å and $|c|$ = 5.33 Å,[23] consistent with the measured value of 5.31 Å.[47] The symmetry breaking we find here is likely due to a Jahn–Teller distortion of the d^6 Fe(II) octahedral field, which may be averaged out in the real sample. The calculated lattice constants for Fe_2O_3 are $|a|$ = 5.10 Å and $|c|$ = 13.92 Å,[23] and the corresponding experimental values are $|a|$ = 5.04 Å and $|c|$ = 13.75 Å.[48] More details of structural optimization are given below.

2.1. Band gap center calculations

BGC calculations were performed for the MnO(001), FeO(001), Fe_2O_3(0001), $Fe_2O_3(01\bar{1}2)$, NiO(001), and Cu_2O(111) surfaces. The (001) surface plane was chosen for the rocksalt TMOs because of its stability and non-polarity (that is, no net electric dipole moment normal to the cleavage plane).[40,49–51] The Cu_2O(111) surface was selected since it was found experimentally to be more stable than Cu_2O(001).[52] In hematite, the Fe_2O_3 (0001) and $(01\bar{1}2)$ surfaces have similar surface energies, with the surface energy of the $(01\bar{1}2)$ slightly lower by $\sim$0.1 J/m^2,[40] so we report predictions for both surfaces.

Periodic unit cells containing five-layer thick slabs and 10 Å of vacuum separating slabs from their periodic images were used for the rocksalt TMOs (MnO, FeO, and NiO). The models for MnO and NiO contained eight atoms per layer, which converged the surface energies of MnO and NiO to within 0.01 J/m^2, while FeO required a lateral unit cell with 16 atoms per layer to properly converge its surface energy to within 0.1 J/m^2 due to its rhombohedral distortion.[40] The slab used for the Fe_2O_3(0001) surface was four stoichiometric units thick with a vacuum thickness of 15 Å, and the slab for the Fe_2O_3 $(01\bar{1}2)$ surface was three stoichiometric units thick with a vacuum of 10 Å. Further computational details on the predicted equilibrium surface structures of iron oxides can be found in ref. 40. Five tri-layers, each consisting of a layer of four Cu atoms sandwiched between two O atoms in the lateral unit cell, along with a 10 Å vacuum layer, were needed to converge the surface energy of Cu_2O to within 0.01 J/m^2. The (001) interlayer spacings in MnO, FeO, and NiO are $\sim$2.2 Å, $\sim$2.2 Å, and $\sim$2.1 Å, respectively, stoichiometric layers of Fe_2O_3 are respectively $\sim$2.2 Å and $\sim$3.2 Å thick for the (0001) and $(01\bar{1}2)$ slabs, and one stoichiometric layer for Cu_2O is $\sim$2.2 Å thick. Consequently, the slab models of all the oxides are fairly similar in thickness: $\sim$8.5–9 Å for MnO, FeO, NiO, and Fe_2O_3(0001), $\sim$9.5 Å for Fe_2O_3 $(01\bar{1}2)$, and $\sim$11 Å for Cu_2O.

Slabs for FeO, Fe_2O_3, and NiO were initially constructed using the bulk primitive cell geometries and all ionic positions

were allowed to relax to an equilibrium structure using the DFT + U functional used for each material's bulk calculation. Cu_2O and MnO slabs were constructed using HSE bulk primitive cell geometries, followed by ionic relaxation of the surface slab with the PBE + U functional (with an empirical value of U-J = 6 eV on Cu and the *ab initio* U-J = 5.0 eV on Mn[53]). PBE + U is used for ionic relaxation because it is 1-2 orders of magnitude less expensive than HSE while still accurately reproducing experimental bulk lattice constants (calculated lattice constants with PBE + U are 4.27 Å for Cu_2O and 5.48 Å for MnO). The ion relaxation was stopped when all force components on all ions were less than 0.03 eV/Å.

K-point meshes consistent with those converged for the bulk calculations were used for the surface slabs: gamma-point-centered grids with $4 \times 4 \times 1$ *k*-points for MnO(001), NiO(001) and $Cu_2O(111)$, $2 \times 2 \times 1$ *k*-points for FeO(001), and a $3 \times 3 \times 1$ *k*-mesh for both Fe_2O_3 (0001) and $Fe_2O_3(01\bar{1}2)$. Use of a gamma-point-centered grid is important for determining the BGC in materials with a direct band (such as Cu_2O) or materials where the calculated CBM appears at the gamma point (such as FeO). The value of the BGC was found converged to within 0.03 eV for all materials compared to denser k-meshes.

Finally, the centers of the KS band gaps were calculated at the resulting equilibrium structures of the surfaces. The BGC is located halfway between the KS VBM and the KS CBM eigenvalues calculated for the surface (periodic slab) unit cell. The position of the BGC relative to vacuum was obtained by taking the energy difference of the calculated electrostatic potential in the vacuum region and the energy of the BGC, using the DFT + U, HSE, and PBE0 functionals independently, for comparison purposes.

2.2. Quasiparticle gap calculations

Calculation of the PES/IPES gap was done using a perturbative, non-self-consistent GW method (G_0W_0) on the bulk structures. The full self-consistent GW approach is much more expensive and is known to carry additional approximations (not invoked in the G_0W_0 calculation) that may lead to errors.[54] Indeed, we have shown in a systematic study of the performance of various forms of the GW method applied to hematite (Fe_2O_3) that the most accurate predictions are obtained when one takes care to use as input to G_0W_0 wavefunctions and energies that describe accurately the ground state of the material.[55] Thus, the input wave functions and energies for the G_0W_0 calculation were obtained from calculations on the bulk unit cell using DFT + U or HSE functionals (the corresponding G_0W_0 calculations will henceforth be denoted by DFT + U/G_0W_0 and HSE/G_0W_0).

The bulk geometries used for the G_0W_0 calculations were obtained from relaxation of the ground state structure using each of these functionals for MnO, Fe_2O_3, and Cu_2O. However, for NiO and FeO, only the structure obtained from geometry optimization with *ab initio* DFT + U was considered, as it is much more economical and the results for the other oxides had already demonstrated that DFT + U predicts very similar structures to those obtained with a hybrid functional (*e.g.*, the difference between HSE and DFT + U Cu_2O lattice constants and bond lengths are respectively <0.015 Å and <0.01 Å).

Gamma-point-centered k-point meshes were used in the G_0W_0 calculations: $4 \times 4 \times 4$ for Fe_2O_3 and NiO, and $6 \times 6 \times 6$ for FeO, MnO, and Cu_2O. The calculation of the response function used a gamma-point-centered $2 \times 2 \times 2$ q-point mesh for MnO, FeO, and Fe_2O_3, and a $3 \times 3 \times 3$ q-point mesh for Cu_2O. The number of q-points was not reduced from the k-mesh for NiO, *i.e.*, a $4 \times 4 \times 4$ q-point mesh was used. The converged number of both bands and frequency points was 64 for Cu_2O, and NiO. For MnO, 64 bands and 96 frequency points were used, and for Fe_2O_3, 96 bands and 100 frequency points were needed. The number of bands and frequency points needed for FeO in the DFT + U/G_0W_0 calculation was 80 and in the HSE/G_0W_0 calculation was 64. It was found to be essential in these G_0W_0 calculations to use more than twice the number of bands used in the preceding DFT + U or hybrid functional calculations in order to converge the value of the QP gap. These settings gave QP gaps that were converged to within 0.1 eV.

Finally, the positions of the band edges relative to vacuum were determined by combining surface and bulk calculations. The QP gap was calculated using the bulk unit cell to model PES/IPES inside the crystal whereas the BGC position relative to vacuum was calculated from the surface unit cell to mimic a work function calculation at a surface. The position of the VBM (CBM) was then calculated by subtracting (adding) half the QP gap to the BGC position relative to vacuum (see eqn (2)).

3. Results and discussion

3.1. Position of the band gap center from density functional theory incorporating exact exchange

Let us start by analyzing the position of the KS VBM because it determines, together with the eigenvalue gap, the center of the band gap. The valence band edge positions of the TMOs MnO, FeO, Fe_2O_3, NiO, and Cu_2O were obtained from the calculations on periodic surface slabs described above. The value of the KS VBM was obtained in reference to the electrostatic potential in the vacuum (see the electrostatic potential of FeO as a representative example in Fig. 1).

Table 1 summarizes the KS VBM of these materials obtained using either DFT + U, HSE, or PBE0 functionals. The difference in the VBM value from DFT + U and PBE0 calculations is $\sim$1 eV in all the TMOs except FeO, for which use of the LDA XC produces a different trend. Indeed since HSE and PBE0 use the PBE XC functional as a central component, it makes sense that LDA + U results would not be directly comparable. If instead we compare the PBE + U prediction for FeO (shown in parentheses is the PBE + U result using the LDA + U structure) to HSE and PBE0, the same trend is observed as for the other materials. The KS VBM of FeO calculated with PBE + U is higher than the one calculated with LDA + U. The difference in KS VBM values from HSE and PBE0 calculations is consistently $\sim$0.4 eV. The KS potential obtained with the PBE0 functional strongly binds electrons and increases the energy required to extract an electron from the atoms of

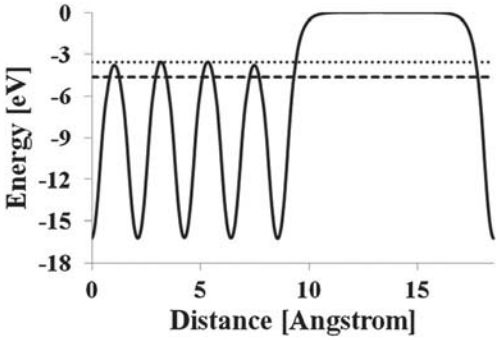

Fig. 1 Electrostatic potential averaged over planes parallel to the surface (solid line), Kohn–Sham valence band maximum (dashed line) and band gap center (dotted line), calculated for FeO(001) using *ab initio* LDA + U theory. The region to the right of ~10 Å is the vacuum region, where the energy is zero (the vacuum level). The energy decreases at the far right where the next periodic image of the FeO slab begins.

Table 1 Calculated values of the Kohn–Sham valence band maximum of transition metal oxides (eV) for three levels of theory, referenced to the vacuum level. The values of U-J used in the DFT + U calculations here are given in section 2. The DFT + U XC functional was PBE for all materials except FeO where LDA was used to determine its structure (see text for details). The PBE + U value for FeO is given in parentheses for comparison

Method	MnO (001)	FeO (001)	Fe_2O_3 (0001)	Fe_2O_3 (01$\bar{1}$2)	NiO (001)	Cu_2O (111)
DFT + U	−4.48	−4.17 (−3.79)	−5.24	−6.14	−5.11	−5.07
HSE	−4.96	−3.91	−5.84	−6.71	−5.71	−5.38
PBE0	−5.28	−4.33	−6.23	−7.09	−6.13	−5.74

the crystal. This emphasizes the significance of the long-range exact exchange expressed in PBE0 that is not accounted for in the HSE functional.[17–19] Because the extraction of an electron from the region of atoms in the crystal to the vacuum region is a long-range process, the long-range nature of the PBE0 functional may be necessary to accurately calculate the KS VBM. By contrast, the DFT + U functional exhibits an exponential dependence with distance, as expressed in the LDA or PBE XC functionals, rather than a long-range Coulomb interaction.

The magnitude of intra-atomic exchange energy contributed to the DFT + U functional by the U-J parameter affects the binding and localization of the d electrons in the transition metal, making it an important parameter for calculating the KS VBM. As seen in Fig. 2a, the KS VBM becomes more negative as the value of the U-J parameter increases, as expected from the theory.[21] The explicit dependence of the KS VBM on the U-J value is expected to be more significant for Mott-Hubbard insulators such as FeO, where the highest occupied band is much more affected because it is localized on the transition metal cation, than for a mixed Mott-Hubbard/charge-transfer insulator such as NiO, where the highest occupied band contains O 2p character. The predicted trends across materials given in Fig. 2a only make sense physically for intermediate values of U-J for reasons we discuss next.

Qualitatively, we expect the KS VBM of MnO and Fe_2O_3 to be more negative than the KS VBM of FeO. High spin Mn(II)

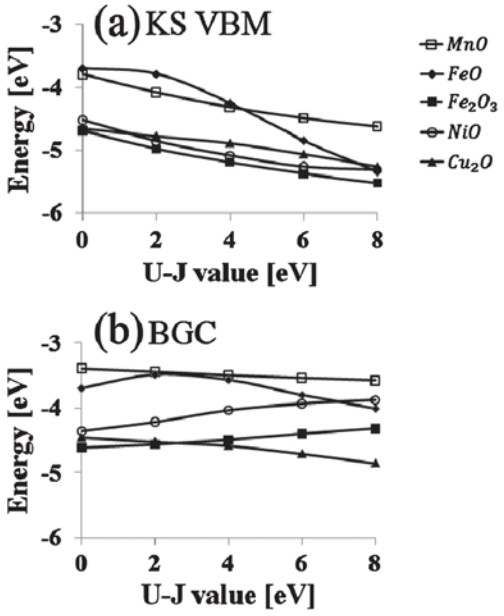

Fig. 2 Dependence of the Kohn–Sham valence band maximum (KS VBM) (a) and band gap center (BGC) (b) on the value of the U-J exchange parameter in DFT + U theory for various transition metal oxides. The slab geometries were first obtained at the DFT + U level of theory using the XC functional and the U-J value given in section 2 for each material and the geometries are then kept fixed as U-J is varied in these calculations. For Fe_2O_3, only values for the basal (0001) plane are shown.

and Fe(III) in MnO and Fe_2O_3 have a half-filled shell with five singly occupied 3d-orbitals that hybridize with oxygen 2p-orbitals at the KS VBM. These electrons are greatly stabilized by the many very large intra-atomic exchange interactions. By contrast, high spin Fe(II) in FeO has a less stable valence configuration of six 3d-electrons due to having two electrons occupy one of the d-orbitals. Ionizing an electron from either MnO or Fe_2O_3 requires more energy (due to the large number of exchange interactions that would be lost) than extracting the one minority spin electron from Fe (II) in FeO (which is destabilized by the presence of the majority spin electron in the same orbital). Examination of Fig. 2a shows that these trends only hold for low-to-intermediate values of U-J such as those found by our *ab initio* procedure.[23]

Using the *ab initio* U-J values given in section 2 for the DFT + U calculations (except for Cu_2O, where an empirical U-J value was used because the *ab initio* value is not yet available), or using hybrid functionals, leads to the KS VBM predictions displayed in Table 1. We can see that the KS VBM do indeed follow the expected trend, with a more negative KS VBM for MnO than for FeO, and an even more negative KS VBM for both surfaces of Fe_2O_3 due to its more contracted d-shell (the more positively charged Fe(III) gives rise to even larger exchange stabilization). NiO and Cu_2O, with their highly contracted d-shells, also exhibit KS VBM values that are qualitatively similar to Fe_2O_3 (0001); the Fe_2O_3 (01$\bar{1}$2) KS VBM appears at more negative values because its surface is oxygen-terminated[40] and the negatively charged oxygens increase the work function compared to the surfaces that have surface cations present.

Table 2 Calculated values of the band gap center for several transition metal oxides (eV) for three different levels of theory, referenced to the vacuum level. See Table 1 caption for more details

Method	MnO (001)	FeO (001)	Fe_2O_3 (0001)	Fe_2O_3 ($01\bar{1}2$)	NiO (001)	Cu_2O (111)
DFT + U	−3.50	−3.54 (−3.13)	−4.48	−5.14	−4.08	−4.70
HSE	−3.49	−2.92	−4.71	−5.33	−3.91	−4.51
PBE0	−3.49	−2.97	−4.72	−5.34	−3.94	−4.51

The center of the KS band gap depends on both the KS VBM and the eigenvalue gap. For the reasons discussed earlier, the KS VBM obeys the relation $E_{VBM}(PBE+U) > E_{VBM}(HSE) > E_{VBM}(PBE0)$. The eigenvalue gap exhibits the opposite trend and depends on the XC functional according to $E_g(PBE+U) < E_g(HSE) < E_g(PBE0)$ due to the increasing amount of Hartree–Fock exchange going from PBE + U to HSE to PBE0 that increases the band gap. Because of these competing trends, we expect the BGC to be rather insensitive to the choice of XC functional. Table 2 shows the BGC calculated with different XC functionals, referenced to the electrostatic potential in the vacuum region (see dotted line in Fig. 1). Indeed, there is only a slight difference in the value of the BGC between different choices of XC functional. Additionally, Fig. 2b illustrates that the BGC depends only modestly on the U-J value, much less than the KS VBM does. It appears that the value of the BGC is rather independent of the choice of XC functional and hence we may conclude that the much less expensive DFT + U theory can be used to compute BGCs in future work without sacrificing accuracy while saving computational time.

The results above show that given a particular surface structure, the BGC is rather insensitive to the choice of XC functional used. However, different XC functionals may affect the predicted surface structure, which in turn may impact the predicted BGC. We therefore also tested the sensitivity of our BGC predictions to using different XC functionals for ionic relaxation at surfaces. We considered MnO and Fe_2O_3, as two extreme cases: rock salt MnO is not expected to exhibit much surface relaxation, while the hematite (corundum structure) surfaces exhibit large surface relaxations. Starting with (001) slabs for MnO constructed from the experimental primitive cell geometry to avoid a bias in the comparison, relaxed surfaces using either the PBE + U or PBE0 functional exhibit no reconstruction, with surface oxygen ions simply moving slightly toward vacuum and surface manganese ions shifted slightly inward. PBE0 BGC values of −3.48 eV and −3.44 eV are obtained for the two surfaces relaxed using PBE + U and PBE0, respectively, and these are nearly the same as those in Table 2 for three different functionals using the PBE + U surface structure. Moving on to hematite, we compared BGCs for the (0001) surface using LDA + U or PBE + U to calculate both the structure and the BGC. The interlayer spacing at the surface differs by only 0.01 Å and < 0.03 Å in subsurface layers for the two XC functionals,[40] leading to an LDA + U BGC of −4.69 eV, within 0.21 eV of the prediction in Table 2 for PBE + U structures and BGCs. Hence, we conclude that equilibrium surface structures obtained from different XC functionals have no effect on the BGC predictions for rock salt materials while introducing a few tenths eV uncertainty into the BGCs for materials exhibiting large surface relaxations.

3.2. Position of the valence band maximum and the conduction band minimum from the G_0W_0 approximation

The positions of the VBM and CBM of MnO, FeO, Fe_2O_3, NiO, and Cu_2O were determined from the above predicted BGCs and the QP gaps computed with a non-self-consistent G_0W_0 calculation discussed next. The energies and wavefunctions used as input for G_0W_0 were obtained by solving the KS-DFT eigenvalue equations with a rational choice for the XC functional, *i.e.*, those found to be most accurate for each material's ground state bulk properties. This corresponds to *ab initio* DFT + U for FeO, Fe_2O_3, and NiO, and HSE for MnO and Cu_2O. Indeed, as mentioned earlier, a systematic study on hematite (Fe_2O_3) showed that G_0W_0 with *ab initio* DFT + U input best matches the experimental PES/IPES energy gap.[55] FeO appears to be an exception since the LDA + 3.7/G_0W_0 QP gap calculated here (1.6 eV) exhibits no increase from the LDA + 3.7 eigenvalue gap.[23] Similar behavior was reported previously for DFT + U/G_0W_0 calculations of FeO and CoO.[56] However, our calculated FeO QP gap refers to the energy difference between a very small peak at the conduction band edge and the VBM, rather than considering the onset of the first substantial peak in the conduction band, which is 0.7 eV higher in energy. The small peak we find at the conduction band edge may correspond to a small intensity optical absorption peak observed at ~1.3 eV, below the onset of a large absorption peak at 2.4 eV,[57] as suggested earlier by other authors who observed a similar peak using LDA + U with a larger value for the U-J parameter than the one used here.[58] If we instead evaluate the QP gap between the rise of the first substantial conduction band peak and the VBM, we obtain values of 2.3 and 3.3 eV respectively for LDA + U/G_0W_0 and HSE/G_0W_0 (the HSE/G_0W_0 QP energy gap between the rise of the small intensity peak and the VBM is 2.25 eV). Final values of our best estimates for the QP gaps are given in Table 3, showing quite reasonable agreement with measurements.[14,57,59–61]

Previously reported GW studies of TMOs include an LDA/G_0W_0 calculation for the QP gap of Cu_2O that disagrees significantly with experiment[62] due to a poor choice of input wavefunction from DFT-LDA (poor for late TMOs, as noted earlier). Other methods for calculating the QP gap of TMOs, including LDA + U/G_0W_0,[56] HSE/G_0W_0[63] or a fully

Table 3 Experimental band gaps (all from photoemission/inverse photoemission except FeO, which is from optical absorption) and calculated quasiparticle band gaps of various first row transition metal oxides (given in eV). The calculated values are obtained by the G_0W_0 approach, using input from *ab initio* DFT + U for Fe_2O_3, FeO, and NiO, and from HSE for MnO and Cu_2O

	MnO	FeO	Fe_2O_3	NiO	Cu_2O
Calc.	4.13	2.3	3.08	3.60	2.17
Exp.	3.9 ± 0.4[59]	2.4[57]	2.6 ± 0.4[60]	4.0 ± 0.6[14]	2.1 ± 0.1[61]

self-consistent GW calculation[62,64] frequently agree reasonably well with experiment. LDA + U/G_0W_0 calculations were performed for a few transition metal oxides,[56] where the U-J parameter was obtained from constrained DFT, giving similar results to the ones calculated here by DFT + U/G_0W_0 for NiO. The LDA + U/G_0W_0 method[56] for MnO and FeO gives a small gap compared to experiment. HSE/G_0W_0 calculations for MnO and FeO,[63] using a different screening parameter value than the recommended 0.2 Å for the short range exact exchange,[18] gave lower QP gaps than the ones we calculated because our work includes a larger portion of short range exact exchange. The HSE/G_0W_0 calculations for MnO described in ref. 63 gives a QP gap ~0.7 eV smaller than the result given here, however both are within the experimental range of gaps observed. The HSE/G_0W_0 calculation done here for FeO is essentially the same (within 0.05 eV) as the one given in ref. 63. A similar HSE/G_0W_0 calculation for NiO[63] gives a QP gap ~1 eV higher than our PBE + U/G_0W_0 result, but still is within the experimental range of energy gaps. The more expensive, fully self-consistent GW approximation for NiO and MnO[64] yields similar results to the HSE/G_0W_0 calculation in ref. 63. The fully self-consistent GW for Cu_2O gives a QP gap ~0.2 eV lower than our result.[62] While both the fully self-consistent GW and our HSE/G_0W_0 calculation for the QP gap of Cu_2O agree with the range of experimental values available, our result agrees with the more commonly quoted experimental value of 2.17 eV.[62]

With the QP gap in hand, the VBM (CBM) was calculated by subtracting (adding) half of the QP gap from (to) the BGC obtained using the DFT + U functional (see eqn (2)). The VBM and CBM values of MnO, FeO, Fe_2O_3, NiO, and Cu_2O are reported in Tables 4 and 5, respectively, showing varying agreement with the large range of experimental values available. Both the VBM and CBM calculation for MnO lie higher than experiment, arising from the predicted position of its BGC (since the QP gap is in excellent agreement with experiment). However, this way of calculating the VBM, from *ab initio* DFT + U BGCs (referenced to the vacuum level *via* periodic slab calculations) and bulk crystal G_0W_0 QP gaps, in most cases significantly improves agreement with experiment compared to the conventional KS VBM calculation, when we compare these methods at the same *ab initio* DFT + U level of theory (compare Table 1 and Table 4). The exception is Cu_2O, where we regard the close agreement of the DFT + U KS VBM with experiment as fortuitous. For all the other materials, our scheme has a further advantage of computational efficiency, since a very expensive hybrid functional (PBE0) must be employed in a slab calculation of the KS VBM to approach the experimental range of band edge values. Even if the latter theory is used, the VBM values calculated from the BGC and QP gaps are more accurate in most cases. Indeed, any success of the PBE0 functional in obtaining KS-VBM results that resemble the VBM calculated according to our scheme may be attributed to cancellation of the incorrect convexity of the XC functional by adding exact exchange.[65] Finally, we observe that the KS VBM calculated with the HSE functional is accidentally successful in some cases. The HSE KS VBM of Cu_2O agrees best with experiment and for Fe_2O_3 and NiO, the HSE KS VBM is within the large experimental range.

The experimental values for VBM shown in Table 4 were deduced from PES, Kelvin probe measurements, and electrochemical experiments under a variety of conditions and sample preparation methods. The variations in values attest to the difficulty in obtaining accurate values for the pure, defect-free materials. In addition to the approximations inherent in our scheme that lead to inaccuracies, discrepancies between theory and experiment are also due to the presence of imperfections in the samples and the measurements (*e.g.*, the known non-stoichiometry of FeO and Cu_2O, *etc.*). The experimental VBM of MnO(001) was obtained from ultrahigh vacuum PES.[6] The VBMs of FeO and polycrystalline Fe_2O_3 were obtained from work function measurements by the Kelvin probe method under controlled oxygen activity.[7,8] The work function of Fe_2O_3 (0001) was also measured by PES,[9] as was that of single crystal NiO(001).[10,11] The VBM of polycrystalline Cu_2O was obtained from an electrochemical experiment at pH = 12.85.[12] Please see notes in ref. 7–12 for further information. The experimental values of the CBM shown in Table 5 were estimated by adding the measured band gap to the experimental VBM. The band gaps were all PES/IPES gaps except for FeO in which only the optical gap has been measured.

Various VBM calculations have been performed for the single-Fe-terminated Fe_2O_3(0001) surface that we studied here (our results for the $(01\bar{1}2)$ surface are the first available, to our knowledge). All-electron full-potential linearized augmented plane wave DFT-GGA calculations predict a VBM of −4.3 eV;[66] as expected, PAW-DFT-GGA calculations yielded a similar result of −4.0 eV.[67] DFT calculations with the hybrid B3LYP XC functional on point-charge-embedded Fe_2O_3 clusters yield a VBM of −6.7 eV.[68] It is not surprising that the VBM calculated with pure DFT are much higher than our *ab initio* DFT + U/G_0W_0 based prediction of −6.0 eV (Table 4), since the self-interaction error in DFT-GGA artificially overly delocalizes the electrons in the attempt to reduce the too-large electron-electron repulsion, leading to a work function that is more reminiscent of a metal (~4 eV) than a metal oxide. By contrast, our prediction is closer to the earlier prediction obtained using the B3LYP XC functional, which is sensible since

Table 4 Experimental and calculated values of the valence band maximum of transition metal oxides (eV) using eqn (2) (calculated from the DFT + U band gap centers of Table 2 and the quasiparticle gaps of Table 3)

	MnO (001)	FeO (001)	Fe_2O_3 (0001)	Fe_2O_3 $(01\bar{1}2)$	NiO (001)	Cu_2O (111)
Calc.	−5.57	−4.7	−6.02	−6.68	−5.88	−5.79
Exp.	−7.5 ± 0.8[6]	−(4.7−6.8)[7]	−(5.9−8.6)[8,9]		−(4.8−5.5)[10,11]	−5.25[12]

Table 5 Experimental and calculated values of the conduction band minimum of transition metal oxides (eV) using eqn (2). See text for more details

	MnO (001)	FeO (001)	Fe_2O_3 (0001)	Fe_2O_3 (01$\bar{1}$2)	NiO (001)	Cu_2O (111)
Calc.	−1.44	−2.4	−2.94	−3.60	−2.28	−3.62
Exp.	-3.6 ± 1.2[5,59]	−(2.3−4.4)[7,57]	−(3.3−5.6)[9,60]		−(0.2−2.1)[11,14]	-3.15 ± 0.1[12,61]

both calculations have reduced self-interaction error and thus provide a better description of the TMO.

Lastly, we note that the GW approach has been suggested as an alternative means to calculate the band edge positions, as demonstrated on aluminum.[69] However, such calculations are far more expensive than the procedure described here.

3.3. Feasibility of fuel production

The ability of a material to perform redox reactions at its surface depends on the position of its band gap edges relative to the free energies of the reactions of interest. The reactions are thermodynamically favorable if their free energies are located within the band gap energy region. That is, the conditions for thermodynamic favorability of the reduction and oxidation reactions are

$$E_{\mathrm{VBM}} < E_{\mathrm{ox}} \quad (3a)$$

$$E_{\mathrm{red}} < E_{\mathrm{CBM}}, \quad (3b)$$

where E_{red} and E_{ox} are the free energies (for transferring a single mole of electrons or holes) of the reduction and oxidation reactions, respectively.

Fig. 3 shows the calculated band edges of TMOs together with selected redox reaction potentials at pH = 7. Reduction reactions that are of practical significance are those that produce fuels like hydrogen *via* the reduction reaction in water splitting where water is simultaneously oxidized to form O_2. Other reduction reactions that produce fuels or fuel precursors such as methane, methanol, and formic acid use CO_2 as a reactant, which of course has the nontrivial side benefit of slowing the accumulation of CO_2 in the atmosphere. As can be seen in the figure, most of these redox potentials for reducing water and carbon dioxide lie within the band gaps of MnO, Fe_2O_3, NiO, and Cu_2O and therefore these materials are potentially promising for solar-based fuel production.

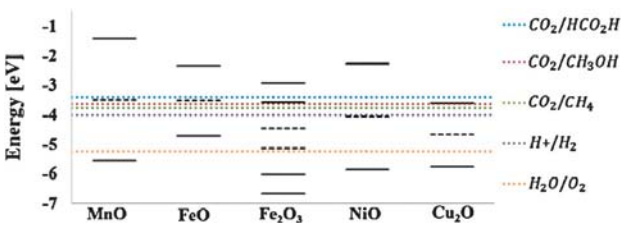

Fig. 3 Best estimates of predicted band edge positions (solid black lines) and band gap centers (dashed black lines) in comparison with measured redox potentials of water splitting and CO_2 reduction reactions producing methane, methanol and formic acid at pH = 7. Two values for each band edge and band gap center are shown for Fe_2O_3 for the two different crystal facets, with the (01$\bar{1}$2) surface consistently at more negative energies.

However, only the reduction reaction free energies are positioned within the band gap of FeO and thus FeO cannot be used for the oxidation of water.

Of course, other characteristics of these materials may hinder their efficacy as photocatalysts or photoelectrodes. First, it is well known that bulk FeO is thermodynamically stable only above 590 °C, much higher than the boiling point of water, which is an essential component of the solution in the electrochemical cell.[70] A potential solution to this problem involves alloying FeO with other materials; we are pursuing this idea at present. Secondly, although MnO and NiO do not absorb sunlight efficiently because of their large band gaps, we have recently discovered that alloying with another metal oxide can reduce their band gap to absorb in the visible range of the solar spectrum. This work will be reported elsewhere.

Photocatalytic water splitting by Cu_2O has been observed experimentally,[71] although some debate has been expressed regarding its ability to oxidize water without being stirred.[72] Presumably the stirring helps mass transport (*e.g.*, displacing hydrogen and oxygen gas bubbles from the surface). Experiments on the photocatalytic activity of Fe_2O_3 show that this material is capable of oxidizing water but is incapable of reducing it without an external bias or addition of fluoride.[73] Although the VBM and CBM alignments of the slightly more stable (01$\bar{1}$2) surface shows better agreement with measurements than those of the (0001) surface, the CBM of the (01$\bar{1}$2) is still higher by ~0.4 eV compared to the free energy of water reduction. The discrepancy between our calculations and experiments likely arises from the fact that our slab model contains vacuum and no solvent, so effects such as how solvent and pH alter the surface structure and band edges were not modeled. For example, it is known that hematite has a hydroxylated surface layer in aqueous solution.[74,75] Therefore, one may expect that extending our model to include hydroxylation and water coverage of hematite will change both surface chemistry and band edges. However, our preliminary calculations show that the BGC of hydroxylated hematite is higher by ~0.2 eV than the BGC position for non-hydroxylated hematite, and that water covered hydroxylated hematite has the same BGC as non-hydroxylated hematite. These findings are consistent with the experimental observation of a moderate decrease in the work function upon increasing water coverage.[9] The experimental value for the BGC is lower than the calculated BGC of both non-hydroxylated hematite and hydroxylated hematite, indicating that additional effects such as pH and band bending at the semiconductor-liquid junction are likely to be involved. We leave these considerations for future work.

The band edge energies of various oxide semiconductors have been shown experimentally to be linearly dependent on

pH, with a slope of approximately 0.059 V per pH unit,[76] just as found for the pH dependence of all redox reaction free energies.

$$E_{\mathrm{VBM(CBM)}}(\mathrm{pH}) = E_{\mathrm{VBM(CBM)}}(\mathrm{pH_{PZC}}) + 0.059\cdot(\mathrm{pH} - \mathrm{pH_{PZC}}) \quad (4)$$

Our calculated band edges may be considered to be at the point of zero charge, $E_{\mathrm{VBM(CBM)}}(\mathrm{pH_{PZC}})$ since we are considering neutral surfaces in vacuum. Hence in principle we should compare our band edges to the redox free energies at the pH corresponding to the point of zero charge, denoted here by $\mathrm{pH_{PZC}}$. However, in order to compare all materials and reactions simultaneously, instead we prefer to compare at a common pH, that of neutral water.

Therefore, we might improve our comparison between band edges and redox free energies by calculating the band edge energies at pH = 7 according to the above expression with the experimental $\mathrm{pH_{PZC}}$. For example, the reported values of $\mathrm{pH_{PZC}}$ for NiO are 9.9[77] and 11,[78] corresponding to a VBM of −6.05 eV and −6.12 eV at pH = 7, which do not differ greatly from the VBM value at $\mathrm{pH_{PZC}}$. This approach is limited for other materials because of widely varying reported values for the $\mathrm{pH_{PZC}}$, due to its high sensitivity to experimental conditions such as defects and impurities.[79] Clearly our model is approximate (no solvent present) and therefore the relative positions of the calculated VBM (CBM) and the redox reaction free energies at pH = 7 shown in Fig. 3 are simply the best estimates we can make at present.

We also note that a semi-empirical approach for calculating band edges has been suggested.[80] The disadvantage of this method is that it relies on experimental values of both the band gap and the $\mathrm{pH_{PZC}}$. In practice, only one experimental value for the band gap and for $\mathrm{pH_{PZC}}$ was chosen in ref. 80 from the range of experimentally reported values available for each material. We regard this approach as less than satisfactory; our goal is a method that provides an estimate that does not rely on experimental input, so as to offer a pure comparison between theory and experiment.

4. Conclusions

The positions of valence band maxima (VBM) and conduction band minima (CBM) of the TMOs MnO, FeO, Fe_2O_3, NiO, and Cu_2O were calculated using an approach that combined results from periodic slab calculations for locating the band gap center (BGC) relative to the vacuum level and bulk crystal quasiparticle (QP) gap calculations. This approach has a number of advantages. First, the value of the BGC was shown to be quite insensitive to the choice of XC functional. Therefore, the less computationally expensive DFT + U functional can be used with confidence for calculating the BGC. Second, the VBM is determined more accurately by calculating the BGC and the QP gap than by the traditional approach of calculating the KS VBM from a periodic slab calculation of the vacuum level. Specifically, the DFT + U BGC plus G_0W_0 QP scheme generally produces superior results to using any of the approximate XC functionals to calculate the KS VBM from a periodic slab, including the much more expensive but potentially accurate PBE0 functional. Third, another advantage of calculating the BGC, rather than the KS VBM as conventionally done, is that this approach is based on a formally exact theorem. Fourth, the *ab initio*-calculated observables of our scheme, including the BGC and the QP gap, are directly comparable to experimentally measured observables, whereas the KS VBM is only an eigenstate of the KS single particle equation and does not have the physical meaning of the material's VBM. Fifth, *ab initio* DFT + U and hybrid DFT served as input for non-self-consistent G_0W_0 calculations of the QP gap, which showed overall excellent agreement with experimental band gap values. Unfortunately, it is difficult to assess the accuracy of calculating band edge positions with slab models due to the lack of precise experimental values; we hope this work will encourage further experimental work on these materials.

The calculated band edge positions were compared to reduction potentials of reactions that produce hydrogen, methane, methanol, and formic acid, and to the oxidation potential of water. MnO, Fe_2O_3, NiO, and Cu_2O were shown to be promising parent materials for water splitting and a number of CO_2 reduction reactions since both reduction and oxidation reaction potentials appear within their band gap. The band gap of FeO does not span both reactions and therefore FeO should not be considered for oxidation of water.

Ongoing work is addressing other drawbacks of these materials, including optimization of band gaps, charge transport, and phase stability, *via* mixed oxide phases and doping. Effects that have not been considered in the models and which should be addressed in future work include the existence of vacancies in the materials and band edge dependence on the adsorption of reactive and solvent species on the surface.

Acknowledgements

E.A.C. thanks the U.S. Air Force Office of Scientific Research and the U.S. Department of Energy, Basic Energy Sciences for funding. This research used resources of the National Energy Research Scientific Computing Center, which is supported by the Office of Science of the U.S. Department of Energy under Contract No. DE-AC02-05CH11231. This work was supported in part by a grant of computer time from the DOD High Performance Computing Modernization Program at the NAVY DSRC. E. A. C. also thanks Dr Lucia Reining for illuminating discussions about the GW method and the importance of high quality ground state input. Research leading to these results also received funding from the *European Union Seventh Framework Programme* (*FP7/2007-2013*) *under grant agreement* no. [254227] to M.C.T. M.C.T. also acknowledges the Sara Lee Schupf Award from the Weizmann Institute and the New England Fund stipend from the Technion. M.C.T. also wishes to thank Dr Rafael Jaramillo from Harvard University and Dr Jens Meyer from Princeton University for discussions on the experimental data.

Notes and references

1 B. Coelho, A. C. Oliveira and A. Mendes, *Energy Environ. Sci.*, 2010, **3**, 1398.
2 M. X. Tan, P. E. Laibinis, S. T. Nguyen, J. M. Kesselman, C. E. Staton and N. S. Lewis, *Principles and Applications of*

Semiconductor Photoelectrochemistry, ed. K. D. Karlin, Progress in Inorganic Chemistry, John Wiley & Sons, Inc., 1994, vol. 41.
3 W. Shockley and H. J. Queisser, *J. Appl. Phys*., 1961, **32**, 510.
4 T. Bak, J. Nowotny, M. Rekas and C. C. Sorrell, *Int. J. Hydrogen Energy*, 2002, **27**, 991.
5 K. H. Wedepohl, in *Composition and abundance of common sedimentary rocks*, ed. K. H. Wedepohl, Handbook of Geochemistry, Spinger-Verlag, Berlin, 1969, vol. I, p. 250.
6 A. Fujimori, N. Kimizuka, T. Akahane, T. Chiba, S. Kimura, F. Minami, K. Siratori, M. Taniguchi, S. Ogawa and S. Suga, *Phys. Rev. B: Condens. Matter*, 1990, **42**, 7580.
7 J. Nowotny and I. Sikora, *J. Electrochem. Soc*., 1978, **125**, 781 The work function of FeO is shown in this paper to be larger than the work function of iron $\phi > 4.7$ eV. As described in the text, the work function of FeO should be smaller than the work function of Fe_2O_3. Since FeO is naturally a *p*-type semiconductor then $0 \leq \Delta \leq 1.2$ eV, where Δ is the difference between the Fermi level and the VBM, as shown in eqn (1). The experimental VBM is evaluated according to eqn (1) with the work function of iron as the lower bound and the work function of Fe_2O_3 as the upper bound.
8 C. Gleitzer, J. Nowotny and M. Rekas, *Appl. Phys. A: Solids Surf*., 1991, **53**, 310. The measured work function ϕ for polycrystalline hematite at the limit of low oxygen pressures was found to be lower from the work function of platinum by 0.3 eV. The work function of platinum is 5.5 ± 0.4 eV according to *CRC Handbook of Physics and Chemistry*, CRC Press, Boca Raton, FL (1996). Hence, the work function ϕ of hematite is 5.2 ± 0.4 eV.
9 R. L. Kurtz and V. E. Henrich, *Phys. Rev. B*, 1987, **36**, 3413. A similar value for the work function of polished and annealed hematite was measured to be $\phi = 5.4 \pm 0.2$ eV. Since hematite is naturally *n*-type, $1.3 \pm 0.2 \leq \Delta \leq 2.6 \pm 0.4$ eV. The experimental VBM is evaluated from the range of $\phi = 4.8$–5.6 eV given in ref. 8 and 9 according to eqn (1). The lower limit of the VBM is calculated from the largest value of ϕ and Δ, and the higher limit is calculated from the lowest value of ϕ and Δ.
10 J. Szuber, *J. Electron Spectrosc. Relat. Phenom*., 1984, **34**, 337. The measured work function ϕ for NiO(001) is 4.35 ± 0.02 eV and the measured Δ is 0.45 eV.
11 J. M. Mckay and V. E. Henrich, *Phys. Rev. B*, 1985, **32**, 6764; The measured work function ϕ for NiO(001) is 4.4 ± 0.1 eV and the measured Δ is 1 eV. The experimental VBM is evaluated according to ref. 10 and 11 and eqn (1).
12 Caballero-Briones J.. M. Artés, I. Díez-Pérez, P. Gorostiza and F. Sanz, *J. Phys. Chem. C*, 2009, **113**, 1028. The measured VBM at pH = 12.85 is −4.9 eV. Since several very different pH_{PZC} values are reported for Cu_2O in ref. 79, the VBM at pH_{PZC} cannot be determined based on experimental pH_{PZC}. The VBM shown in Table 4 was calculated at pH = 7 according to eqn (4).
13 A. Hamnett and A. F. Orchard, in *Photoemission Spectroscopy*, ed. P. Day, Electronic Structure and Magnetism of Inorganic Compounds, Royal Society of Chemistry, 1974, vol. 3.
14 S. Hüfner, *Adv. Phys*., 1994, **43**, 183. The largest reported range for the experimentally measured IPES/PES gap is 3.2–5.7 eV. The value in Table 3 is an estimated range around the more quoted value of 4.3 eV.
15 S. Gutmann, M. A. Wolak, M. Conrad, M. M. Beerbom and R. Schlaf, *J. Appl. Phys*., 2010, **107**, 103705.
16 V. I. Anisimov, F. Aryasetiawan and A. I. Lichtenstein, *J. Phys.: Condens. Matter*, 1997, **9**, 767.
17 J. Heyd, G. E. Scuseria and M. Ernzerhof, *J. Chem. Phys*., 2003, **118**, 8207.
18 J. Heyd, G. E. Scuseria and M. Ernzerhof, *J. Chem. Phys*., 2006, **124**, 219906.
19 J. P. Perdew, M. Ernzerhof and K. Burke, *J. Chem. Phys*., 1996, **105**, 9982.
20 V. I. Anisimov, J. Zaanen and O. K. Andersen, *Phys. Rev. B: Condens. Matter*, 1991, **44**, 943.
21 S. L. Dudarev, G. A. Botton, S. Y. Savrasov, C. J. Humphreys and A. P. Sutton, *Phys. Rev. B: Condens. Matter Mater. Phys*., 1998, **57**, 1505.
22 N. J. Mosey and E. A. Carter, *Phys. Rev. B: Condens. Matter Mater. Phys*., 2007, **76**, 155123.
23 N. J. Mosey, P. Liao and E. A. Carter, *J. Chem. Phys*., 2008, **129**, 014103.
24 M. C. Payne, M. P. Teter, D. C. Allan, T. A. Arias and J. D. Joannopoulos, *Rev. Mod. Phys*., 1992, **64**, 1045.
25 W. Liu, W. T. Zheng and Q. Jiang, *Phys. Rev. B: Condens. Matter Mater. Phys*., 2007, **75**, 235322.
26 G. Onida, L. Reining and A. Rubio, *Rev. Mod. Phys*., 2002, **74**, 601.
27 H. Xiang, S.-H. Wei and X. G. Gong, *J. Phys. Chem. C*, 2009, **113**, 18968.
28 M. J. Rutter and J. Robertson, *Phys. Rev. B: Condens. Matter*, 1998, **57**, 9241.
29 J. P. Perdew and M. Levy, *Phys. Rev. Lett*., 1983, **51**, 1884.
30 J. F. Janak, *Phys. Rev. B*, 1978, **18**, 7165.
31 W. G. Aulbur, L. Jonsson and J. W. Wilkins, *Solid State Phys*., 2000, **54**, 1.
32 O. Bengone, M. Alouani, P. Blochl and J. Hugel, *Phys. Rev. B: Condens. Matter*, 2000, **62**, 16392.
33 G. Kresse and J. Hafner, *Phys. Rev. B: Condens. Matter*, 1993, **47**, 558.
34 G. Kresse and J. Furthmüller, *Comput. Mater. Sci*., 1996, **6**, 15.
35 M. Cococcioni and S. de Gironcoli, *Phys. Rev. B: Condens. Matter Mater. Phys*., 2005, **71**, 035105.
36 T. Cai, H. Han, Y. Yu, T. Gao, J. Du and L. Hao, *Phys. B*, 2009, **404**, 89.
37 N. Alidoust and E. A. Carter, to be published.
38 G. Kresse and D. Joubert, *Phys. Rev. B: Condens. Matter Mater. Phys*., 1999, **59**, 1758.
39 P. Blöchl, *Phys. Rev. B: Condens. Matter*, 1994, **50**, 17953.
40 P. Liao and E. A. Carter, *J. Mater. Chem*., 2010, **20**, 6703.
41 O. Jepsen and O. K. Andersen, *Solid State Commun*., 1971, **9**, 1763.
42 G. Lehmann and M. Taut, *Phys. Status Solidi B*, 1972, **54**, 469.
43 P. Blöchl, O. Jepsen and O. K. Andersen, *Phys. Rev. B: Condens. Matter*, 1994, **49**, 16223.
44 B. Morosin, *Phys. Rev*., 1970, **B1**, 236.
45 F. Fiévet, P. Germi, F. De Bergevin and M. Figlarz, *J. Appl. Crystallogr*., 1979, **12**, 387.
46 W. G. Wickoff, *Crystal Structures*, Wiley-Interscience, New York, 1960, vol. 1.
47 C. A. McCammon and L. Liu, *Phys. Chem. Miner*., 1984, **10**, 106.
48 L. W. Finger and R. M. Hazen, *J. Appl. Phys*., 1980, **51**, 5362.
49 M. Prutton, J. A. Walker, M. R. Welton-Cook, R. C. Felton and J. A. Ramsey, *Surf. Sci*., 1979, **89**, 95.
50 P. W. Tasker and D. M. Duffy, *Surf. Sci*., 1984, **137**, 91.
51 W. S. Abdel Halim and A. S. Shalabi, *Solid State Commun*., 2002, **124**, 67.
52 Z. Zheng, B. Huang, Z. Wang, M. Guo, X. Qin, X. Zhang, P. Wang and Y. Dai, *J. Phys. Chem. C*, 2009, **113**(32), 14448.
53 D. K. Kanan and E. A. Carter, to be published.
54 M. Shishkin and G. Kresse, *Phys. Rev. B: Condens. Matter Mater. Phys*., 2007, **75**, 235102.
55 P. Liao and E. A. Carter, *Phys. Chem. Chem. Phys*., 2011, DOI: 10.1039/C1CP20829B.
56 H. Jiang, R. I. Gomez-Abal, P. Rinke and M. Scheffler, *Phys. Rev. B: Condens. Matter Mater. Phys*., 2010, **82**, 045108.
57 I. Balberg and H. L. Pinch, *J. Magn. Magn. Mater*., 1978, **7**, 12. The only experimentally available energy gap of FeO is the optical absorption gap.
58 I. I. Mazin and V. I. Anisimov, *Phys. Rev. B: Condens. Matter*, 1997, **55**, 12822.
59 J. van Elp, R. H. Prtze, H. Eskes, R. Berger and G. A. Sawatzky, *Phys. Rev. B: Condens. Matter*, 1991, **44**, 1530.
60 R. Zimmermann, P. Steiner, R. Claessen, F. Reinert, S. Hufner, P. Blaha and P. Dufek, *J. Phys.: Condens. Matter*, 1999, **11**, 1657. The CBM is calculated by adding the experimental band gap given in this reference and the experimental VBM (see ref. 9). The lower limit of the CBM is calculated from the lowest VBM and largest E_g and the upper limit of the CBM is calculated from the highest value for ϕ and largest value for E_g and the case of $\Delta = \frac{1}{2}E_g$ (all other combinations yield values that are within this calculated range for the CBM).
61 S. Brahms, S. Nikitine and J. P. Dahl, *Phys. Lett*., 1966, **22**, 31.
62 F. Bruneval, N. Vast, L. Reining, M. Izquierdo, F. Sirotti and N. Barrett, *Phys. Rev. Lett*., 2006, **97**, 267601.
63 C. Rödl, F. Fuchs, J. Furthmüller and F. Bechstedt, *Phys. Rev. B: Condens. Matter Mater. Phys*., 2009, **79**, 235114.

64 S. V. Faleev, M. van Schilfgaarde and T. Kotani, *Phys. Rev. Lett.*, 2004, **93**, 126406.
65 A. Cohen, P. Mori-Sánchez and W. Yang, *Science*, 2008, **321**, 792.
66 X.-G. Wang, W. Weiss, Sh. K. Shaikhutdinov, M. Ritter, M. Petersen, F. Wagner, R. Schlögl and M. Scheffler, *Phys. Rev. Lett.*, 1998, **81**, 1038.
67 J. Jin, X. Ma, C.-Y. Kim, D. E. Ellis and M. J. Bedzyk, *Surf. Sci.*, 2007, **601**, 3082.
68 E. Batista and R. A. Friesner, *J. Phys. Chem. B*, 2002, **106**, 8136.
69 S. V. Faleev, O. N. Mryasov and T. R. Mattson, *Phys. Rev. B: Condens. Matter Mater. Phys.*, 2010, **81**, 205436.
70 L. S. Darken and R. W. Gurry, *J. Am. Chem. Soc.*, 1945, **67**, 1398.
71 M. Hara, T. Kondo, M. Komoda, S. Ikeda, K. Shinohara, A. Tanaka, J. N. Kondo and K. Domen, *Chem. Commun.*, 1998, 357.
72 P. E. de Jongh, D. Vanmaekelbergh and J. J. Kelly, *Chem. Commun.*, 1999, 1069.
73 Y.-S. Hu, A. Kleiman-Shwarsctein, G. D. Stucky and E. W. McFarland, *Chem. Commun.*, 2009, 2652.
74 K. S. Tanwar, C. S. Lo, P. J. Eng, J. G. Catalano, D. A. Walko, G. E. Brown Jr., G. A. Waychunas, A. M. Chaka and T. P. Trainor, *Surf. Sci.*, 2007, **601**, 460.
75 T. P. Trainor, A. M. Chaka, P. J. Eng, M. Newville, G. A. Waychunas, J. G. Catalano and G. E. Brown Jr., *Surf. Sci.*, 2004, **573**, 204.
76 J. M. Bolts and M. S. Wrighton, *J. Phys. Chem.*, 1976, **80**, 2641.
77 R. J. Crawford, I. H. Harding and D. E. Mainwaring, *Langmuir*, 1993, **9**, 3050.
78 R. J. Crawford, I. H. Harding and D. E. Mainwaring, *J. Colloid Interface Sci.*, 1996, **181**, 561.
79 M. Kosmulski, *Chemical properties of material surfaces*, CRC press, 2001, ch. 3.
80 Y. Xu and M. A. A. Schoonen, *Am. Mineral.*, 2000, **85**, 543.

